Supporting information

Rational Design of $Ti_3C_2T_x$ MXene Inks for Conductive, Transparent Films

Tiezhu Guo[1,2], Di Zhou[1*], Shungui Deng[2,3], Mohammad Jafarpour[2,3], Jonathan Avaro[4,5], Antonia Neels[6,7], Jakob Heier[2*], Chuanfang (John) Zhang[8*]

1 Key Laboratory of Multifunctional Materials and Structures, Ministry of Education, School of Electronic Science and Engineering, Xi'an Jiaotong University, Xi'an 710049, Shaanxi, China

2 Laboratory for Functional Polymers, Empa, Swiss Federal Laboratories for Materials Science and Technology, Überlandstrasse 129, CH-8600, Dübendorf, Switzerland

3 Institute of Materials Science and Engineering, Ecole Polytechnique Federale de Lausanne (EPFL), Station 12, CH-1015 Lausanne, Switzerland

4 Center for X-ray Analytics, Empa, Swiss Federal Laboratories for Materials Science and Technology, Lerchenfeldstrasse 5, CH-9014, St. Gallen, Switzerland.

5 Biomimetic Membranes and Textile, Empa, Swiss Federal Laboratories for Materials Science and Technology, Lerchenfeldstrasse 5, St. Gallen CH-9014, Switzerland.

6 Center for X-ray Analytics, Empa, Swiss Federal Laboratories for Materials Science and Technology, Überlandstrasse 129, CH-8600, Dübendorf, Switzerland.

7 Department of Chemistry, University of Fribourg, Chemin du Musée 9, CH-1700, Fribourg, Switzerland

8 College of Materials Science & Engineering, Sichuan University, Chengdu, 610065, Sichuan, China

[1]Corresponding author (zhoudi1220@mail.xjtu.edu.cn)

[2]Corresponding author (Jakob.Heier@empa.ch)

[3]Corresponding author (chuanfang.zhang@scu.edu.cn)

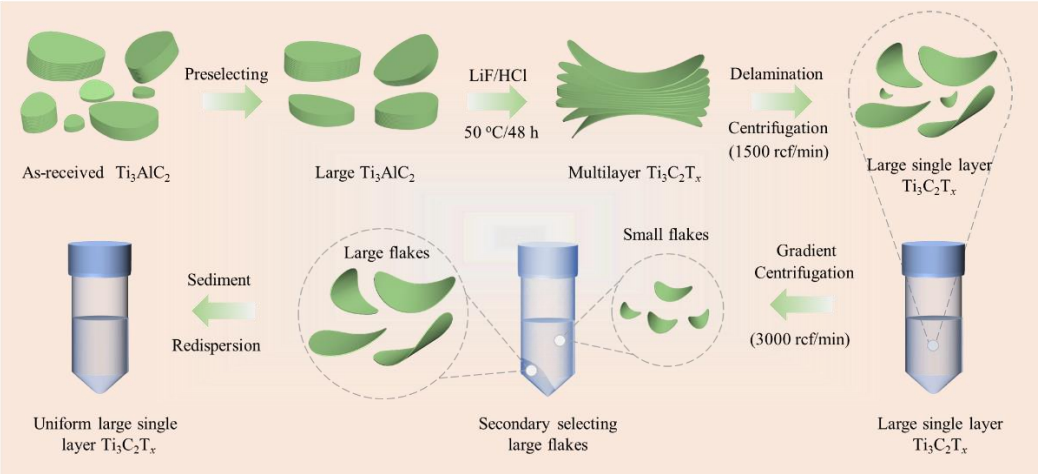

Scheme S1 Schematic illustration of the synthesis process of ultralarge sized $Ti_3C_2T_x$ flakes from the as-received Ti_3AlC_2 phase.

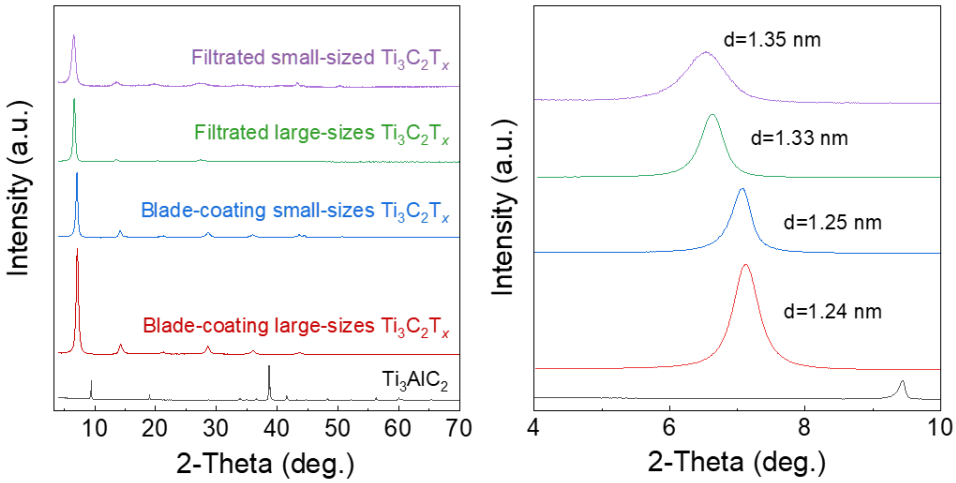

Figure S1 XRD patterns of Ti_3AlC_2, opaque $Ti_3C_2T_x$ films with large-sizes and small-sizes by vacuum-assisted filtration and blade coating.

$Ti_3C_2T_x$ films prepared by blade coating have a smaller interlayer spacing than those of filtrated films. Their interlayer spacing is 1.24 nm (blade-coating large-sized $Ti_3C_2T_x$), 1.25 nm (blade-coating small-sized $Ti_3C_2T_x$), 1.33 nm (filtrated large-sized $Ti_3C_2T_x$), 1.35 nm (filtrated large-sizes $Ti_3C_2T_x$), respectively.

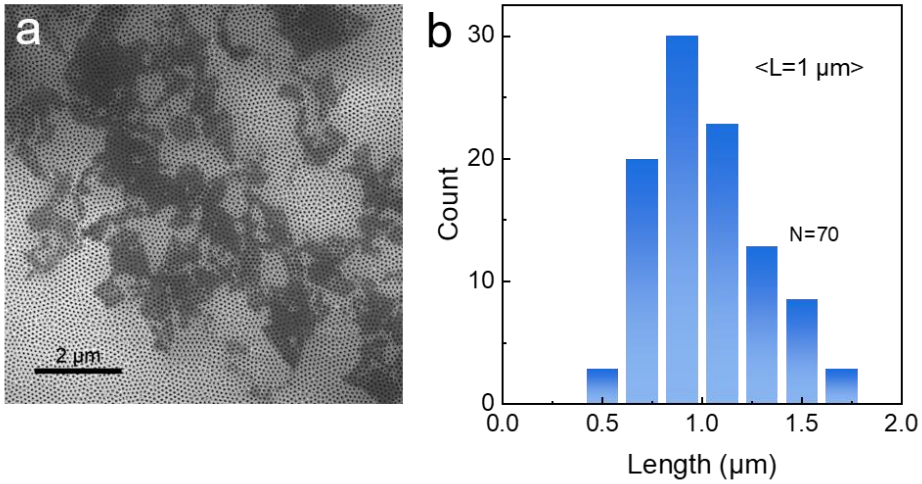

Figure S2 a SEM image of small-sized $Ti_3C_2T_x$ flakes on anodic aluminum oxide (AAO). **b** Histogram of the small-sized $Ti_3C_2T_x$ flakes determined by statistical analysis.

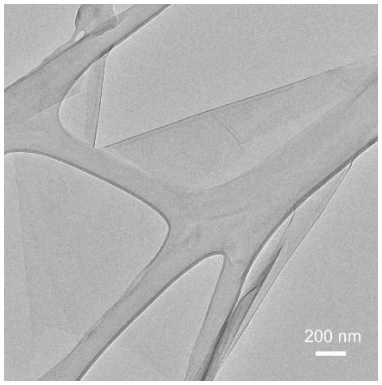

Figure S3 TEM image of a $Ti_3C_2T_x$ flake

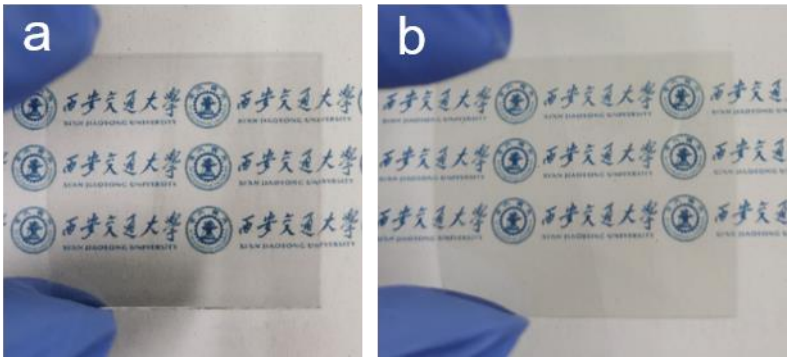

Figure S4 Digital photograph of $Ti_3C_2T_x$ films from large-sizes flakes on glass (**a**, *T*=87%), on PET (**b**, *T*=91%).

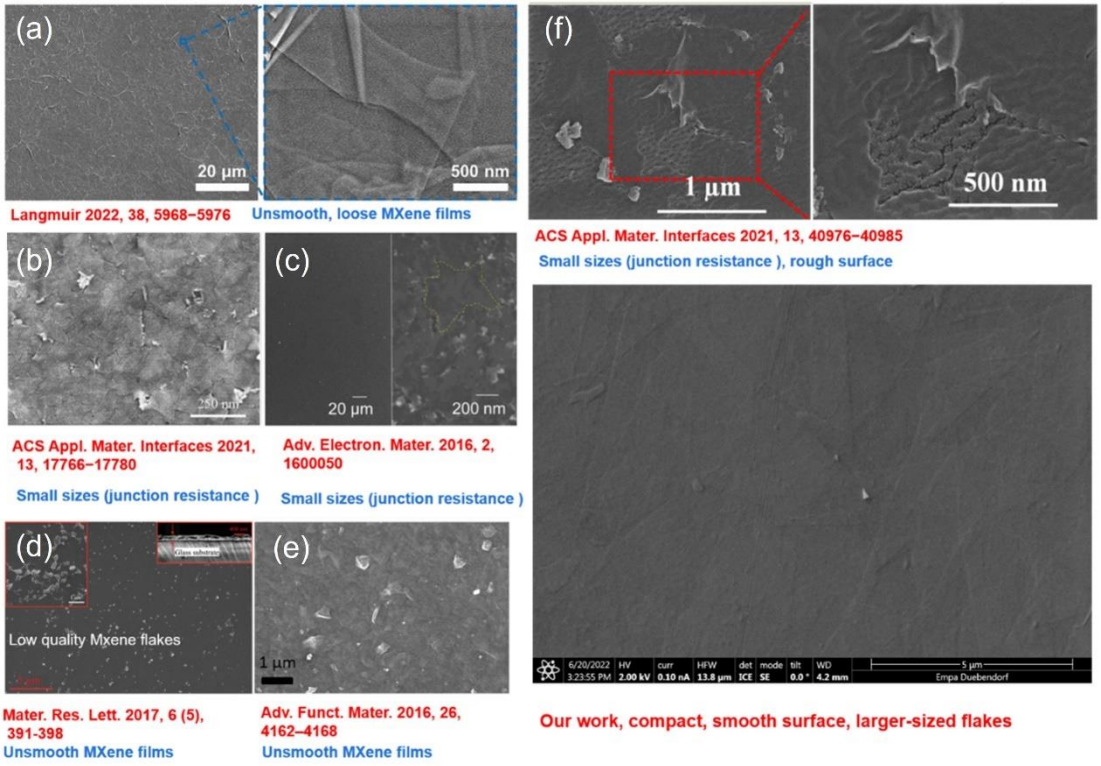

Figure S5 Comparison of SEM images from previously published works with our transparent MXene film. **a** Reproduced with permission.[1] Copyright 2022, American Chemical Society. **b** Reproduced with permission.[2] Copyright 2021, American Chemical Society. **c** Reproduced with permission.[3] Copyright 2016, John Wiley and Sons. **d** Reproduced with permission.[4] Copyright 2017, Taylor & Francis Group. **e** Reproduced with permission.[5] Copyright 2016, John Wiley and Sons. **f** Reproduced with permission.[6] Copyright 2021, American Chemical Society.

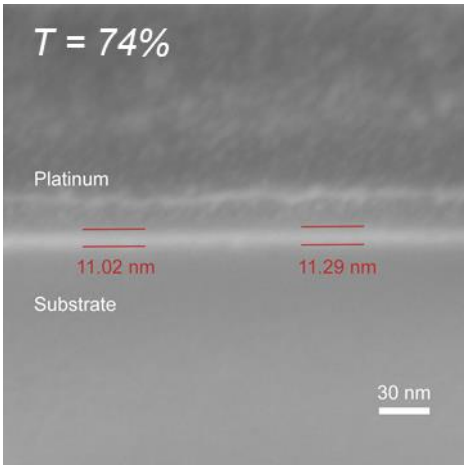

Figure S6 Cross-sectional FIB-SEM image of a blade coated $Ti_3C_2T_x$ film. (T=74%).

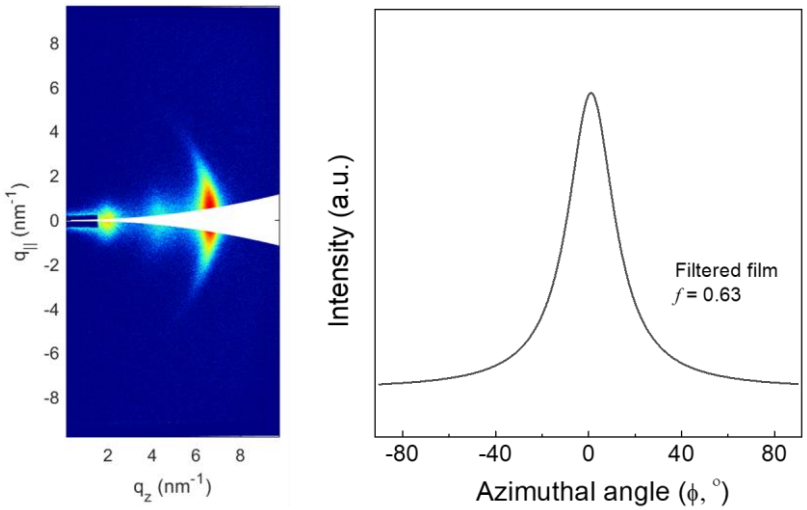

Figure S7 GISAXS measurement of a filtered film (~1 μm). GISAXS detector image showing the (002) peak over q_z. Lorentzian fit of the azimuthal profile for the (002) peak used to determine Herman's degree of orientation.

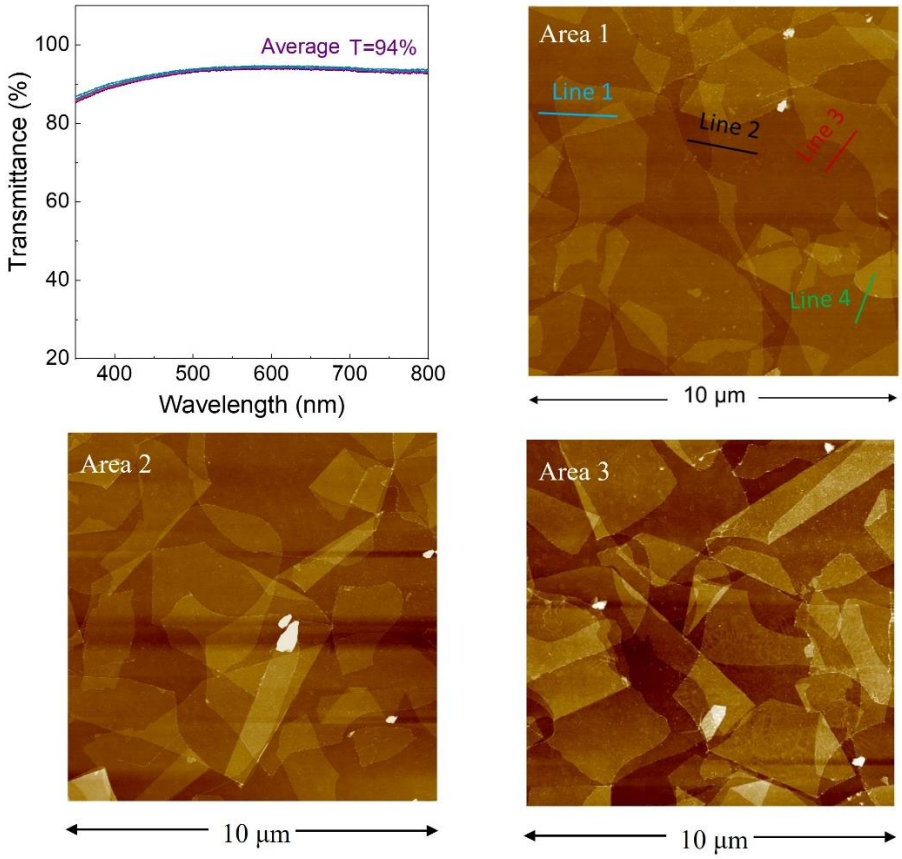

Figure S8 The average transmittance of TCEs and the surface topography of different regions were measured by AFM.

Methods for calculating the number of layers of high transparency films (T=94%), according to the area percentage of the different layers $Ti_3C_2T_x$ flakes in the 10×10 μm area (for the area 1 image). Areas comprising different numbers of layers in Figure 3f are shown with different colors.

Table S1 Calculation of thickness of high transparency film (T=94%).

	Pixel	Percentage (%)	Percentage (%)
Single layer	371 691	37.5%	35.7%
Double layers	495 421	50.0%	47.6%
Triple layers	132 210	13.4%	12.7%
Quadruple layers	15 827	1.6%	1.5%
Substrate (not covered)	25 060	2.5%	2.4%
Actual image pixel	990 024	105%	
Statistical pixel totals	1 040 209		99.9%

Area 1, image pixels: 996×994=990 024

The actual number of pixels counted according to different colors: 1 040 209

Thanks to the pixels at different color boundaries may be counted multiple times, the actual count is slightly higher than the number of pixels in the image.

Method 1:

Single layer: 371 691/990 024 =37.5%

Double layers: 495 421/990 024 =50.0%

Triple layers: 132 210/990 024 =13.4%

Quadruple layers: 15 827/990 024 =1.6%

Substrate: 25 060/990 024 = 2.5%

Layers calculation: 1×0.375+2×0.5+3×0.134+4×0.016=1.84

Percentage of coverage: 100%-2.5%=97.5%

Method 2:

Single layer: 371 691/1 040 209 =35.7%

Double layers: 495 421/1 040 209 =47.6%

Triple layers: 132 210/1 040 209 =12.7%

Quadruple layers: 15 827/1 040 209 =1.5%

Substrate: 25 060/1 040 209 = 2.4%

Layers calculation: 1×0.357+2×0.476+3×0.127+4×0.015=1.75

Percentage of coverage: 100%-2.4%=97.6%

Thus, the thickness of the TCE (T=94%) is 1.8 layers and the coverage is about 98%.

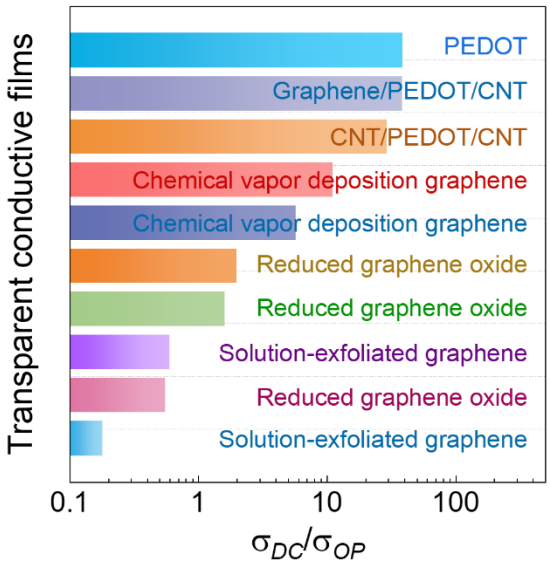

Figure S9 Comparison of σ_{DC}/σ_{op} (FOM_e) of various transparent conductive films, detailed values are presented in Table S2.

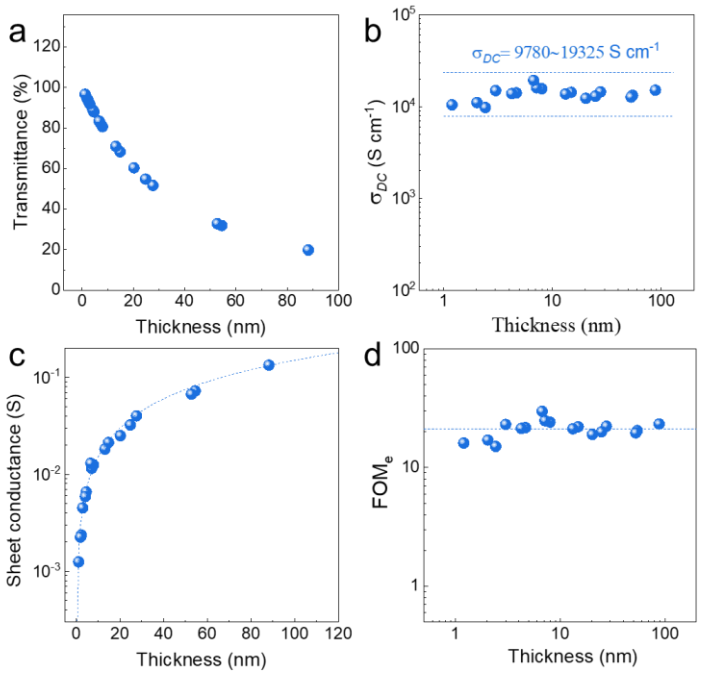

Figure S10 Relationship between $Ti_3C_2T_x$ films thickness and optoelectronic properties. **a** Transmittance, **b** DC conductivity, **c** sheet conductance, **d** Ratio of DC conductivity to optical conductivity.

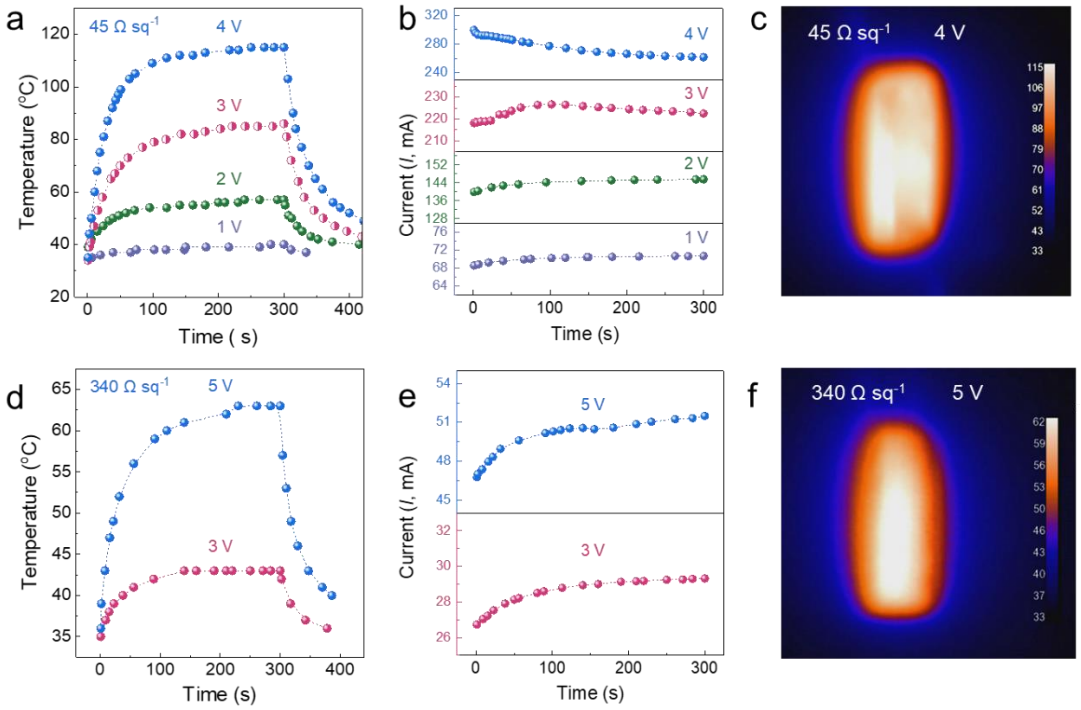

Figure S11 Electrothermal properties of $Ti_3C_2T_x$ films. The time-varying surface temperature of the $Ti_3C_2T_x$ films with 45 Ω sq^{-1} **a)** and 340 Ω sq^{-1} **d)** for different applied voltages. **b, e)** The corresponding current values as a function of time. Infrared radiation (IR) images of the transparent $Ti_3C_2T_x$ films with 45 Ω sq^{-1} **c)** and 340 Ω sq^{-1} **f)**.

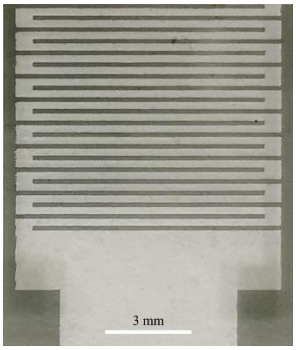

Figure S12 Digital photograph of $Ti_3C_2T_x$-based symmetric micro-supercapacitors

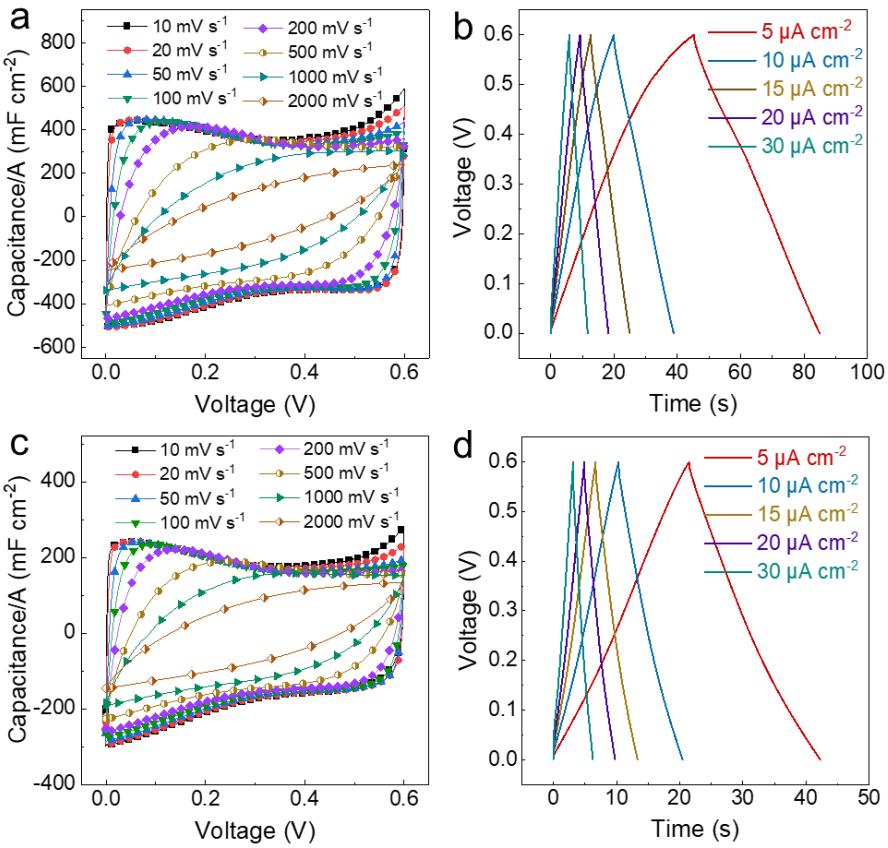

Figure S13 Electrochemical characterization of $Ti_3C_2T_x$ films. Normalized CV curves at various scan rates of **a)** *T*=49%, **c)** T=61%, and GCD curves at different current densities of **b)** T=49%, **d)** T=61%.

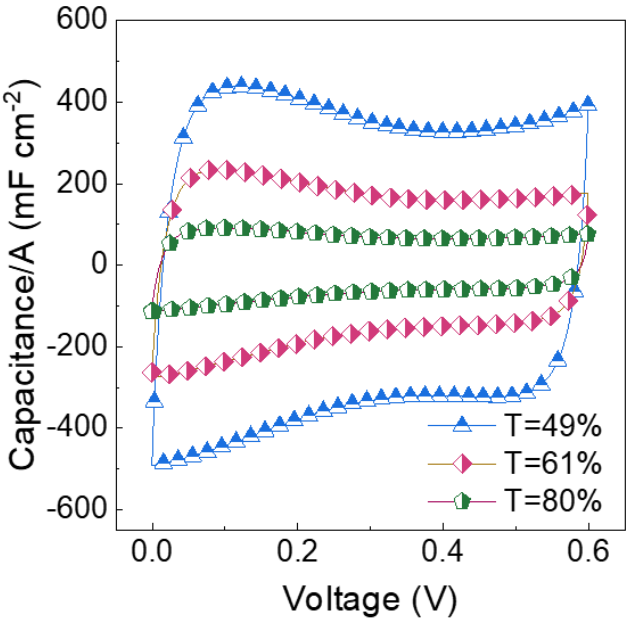

Figure S14 CV curves with different transparency at 100 mV s^{-1}.

Table S2 of **Figure 3b**

Samples	Sizes	Manufacturing technique	Transmittance ($T_{550\ nm}$,%)	Sheet resistance ($\Omega\ sq^{-1}$)	FoM_e	Ref.
$Ti_3C_2T_x$	100~300 nm	Inkjet-printing	24	1500	0.12	2
$Ti_3C_2T_x$	~500 nm	Spray-coating	~51 ~81	~625 ~8160	0.51	3
$Ti_3C_2T_x$	~80 nm	Spin-coating	72 83 90 94	2010 3850 11870 23660	2	7
$Ti_3C_2T_x$	~110 nm	Spin-coating	~72 ~87	~440 ~8900	3.1	8
Ti_2CT_x	~1 μm	Spin-coating	65 80 86 96	128 507 1100 6440	5	4
V_2CT_x	0.5~1 μm	Spin-coating	~50	~67	6.5	9
$Ti_3C_2T_x$	—	Spin-coating	86	330	7.3	5
$Ti_3C_2T_x$	~0.5 μm	Dip-coating	~86	~375	9	10
$Ti_3C_2T_x$	~1.4 μm	Dip-coating	~88	~600	14	
$Ti_3C_2T_x$	~1.4 μm/ Optimizated	Dip-coating	~89 ~92	~320 ~1870	17	
$Ti_3C_2T_x$	1~2 μm	Dip-coating	51 94	40 4300	14	11
$Ti_3C_2T_x$	~3.2 μm	Spin-coating	86 90 94	200 532 1031	15	12
$Ti_3C_2T_x$	12.2 μm	Blade-coating	20	7.5	21	This work
			60	40		
			81	80		
			89	170		
			94	423		

Table S3 of **Figure S9**

Samples	FoM_e	Ref.
PEDOT	39	[13]
Graphene/PEDOT/CNT	38.6	[14]
CNT/PEDOT/CNT	29.18	[15]
CVD-graphene	11.13	[16]
CVD-graphene	5.7	[17]
Reduced graphene oxide	2	[18]
Reduced graphene oxide	1.6	[19]
Solution-exfoliate graphene	0.6	[20]

Reduced graphene oxide	0.55	[21]
Solution-exfoliated graphene	0.18	[22]

Table S4 of **Figure 4c**

Samples	Average electronic conductivity (S cm^{-1})	Ref.
Reduced graphene oxide	550	23
Reduced graphene oxide	1425	24
$Ti_3C_2T_x$	3092	8
Ti_2CT_x	5250	4
$Ti_3C_2T_x$	6500	5
$Ti_3C_2T_x$	7450	12
$Ti_3C_2T_x$	7530	10
$Ti_3C_2T_x$	15000	This work

Table S5 of **Figure 6g**

Samples	Transmittance (T_{550} nm,%)	Capacitance (μF cm^{-2})	Ref.
Graphene Q-dot	93	9.1	25
Graphene networks	84	4.2	26
Wrinkled graphene	60	5.8	27
Graphene film	67	12.4	28
$Ti_3C_2T_x$	88	19	11
	38	283	
$Ti_3C_2T_x$	81	870	12
$Ti_3C_2T_x$	73	192	2
$Ti_3C_2T_x$	49	383.16	This work
	61	189.5	
	80	75.3	

Table S6 of **Figure 6h**

Samples	Transmittance (T_{550} nm, %)	Power density ($\mu W\ cm^{-2}$)	Energy density($\mu Wh\ cm^{-2}$)	Ref.
Graphene film	67	70	0.00047	28
$Ti_3C_2T_x$	88	0.0188	0.00163	11
	38	1.3	0.01	
$Ti_3C_2T_x$	73	0.077	0.0043	2
$Ti_3C_2T_x$	49	1.1496 2.28 5.526 10.608 19.836	0.01916 0.019 0.01842 0.01768 0.01653	This work
	61	0.5682 1.1244 2.733 5.244 9.792	0.00947 0.00937 0.00911 0.00874 0.00816	
	80	0.2256 0.4512 1.098 2.118 3.948	0.00376 0.00376 0.00366 0.00353 0.00329	

References

(1) Huang, L.; Lin, Y.; Zeng, W.; Xu, C.; Chen, Z.; Wang, Q.; Zhou, H.; Yu, Q.; Zhao, B.; Ruan, L.; et al. Highly Transparent and Flexible Zn-$Ti_3C_2T_x$ MXene Hybrid Capacitors. *Langmuir* **2022**, *38*, 5968-5976.

(2) Wen, D.; Wang, X.; Liu, L.; Hu, C.; Sun, C.; Wu, Y.; Zhao, Y.; Zhang, J.; Liu, X.; Ying, G. Inkjet Printing Transparent and Conductive MXene ($Ti_3C_2T_x$) Films: A Strategy for Flexible Energy Storage Devices. *ACS Appl. Mater. Inter.* **2021**, *13*, 17766-17780.

(3) Hantanasirisakul, K.; Zhao, M. Q.; Urbankowski, P.; Halim, J.; Anasori, B.; Kota, S.; Ren, C. E.; Barsoum, M. W.; Gogotsi, Y. Fabrication of $Ti_3C_2T_x$ MXene Transparent

Thin Films with Tunable Optoelectronic Properties. *Adv. Electron. Mater.* **2016**, *2*, 1600050.

(4) Ying, G.; Dillon, A. D.; Fafarman, A. T.; Barsoum, M. W. Transparent, conductive solution processed spincast 2D Ti_2CT_x (MXene) films. *Mater. Res.h Lett.* **2017**, *5*, 391-398.

(5) Dillon, A. D.; Ghidiu, M. J.; Krick, A. L.; Griggs, J.; May, S. J.; Gogotsi, Y.; Barsoum, M. W.; Fafarman, A. T. Highly Conductive Optical Quality Solution-Processed Films of 2D Titanium Carbide. *Adv. Funct. Mater.* **2016**, *26*, 4162-4168.

(6) Kumar, S.; Kang, D.; Nguyen, V. H.; Nasir, N.; Hong, H.; Kim, M.; Nguyen, D. C.; Lee, Y. J.; Lee, N.; Seo, Y. Application of Titanium-Carbide MXene-Based Transparent Conducting Electrodes in Flexible Smart Windows. *ACS Appl. Mater. Inter.* **2021**, *13*, 40976-40985.

(7) Ebrahimi, M.; Mei, C. T. Optoelectronic properties of $Ti_3C_2T_x$ MXene transparent conductive electrodes: Microwave synthesis of parent MAX phase. *Ceram. Int.* **2020**, *46*, 28114-28119.

(8) Mariano, M.; Mashtalir, O.; Antonio, F. Q.; Ryu, W. H.; Deng, B.; Xia, F.; Gogotsi, Y.; Taylor, A. D. Solution-processed titanium carbide MXene films examined as highly transparent conductors. *Nanoscale* **2016**, *8*, 16371-16378.

(9) Ying, G.; Kota, S.; Dillon, A. D.; Fafarman, A. T.; Barsoum, M. W. Conductive transparent V_2CT_x (MXene) films. *FlatChem* **2018**, *8*, 25-30.

(10) Salles, P.; Pinto, D.; Hantanasirisakul, K.; Maleski, K.; Shuck, C. E.; Gogotsi, Y. Electrochromic Effect in Titanium Carbide MXene Thin Films Produced by Dip-Coating. *Adv. Funct. Mater.* **2019**, *29*, 1809223.

(11) Salles, P.; Quain, E.; Kurra, N.; Sarycheva, A.; Gogotsi, Y. Automated Scalpel Patterning of Solution Processed Thin Films for Fabrication of Transparent MXene Microsupercapacitors. *Small* **2018**, *14*, e1802864.

(12) Zhang, C. J.; Anasori, B.; Seral-Ascaso, A.; Park, S. H.; McEvoy, N.; Shmeliov, A.; Duesberg, G. S.; Coleman, J. N.; Gogotsi, Y.; Nicolosi, V. Transparent, Flexible, and Conductive 2D Titanium Carbide (MXene) Films with High Volumetric Capacitance. *Adv. Mater.* **2017**, *29*, 1702678.

(13) Higgins, T. M.; Coleman, J. N. Avoiding Resistance Limitations in High-Performance Transparent Supercapacitor Electrodes Based on Large-Area, High-Conductivity PEDOT:PSS Films. *ACS Appl. Mater. Inter.* **2015**, *7*, 16495-16506.

(14) Wang, T.; Wang, Y. Z.; Jing, L. C.; Zhu, Q.; Ethiraj, A. S.; Geng, W.; Tian, Y.; Zhu, Z.; Meng, Z.; Geng, H. Z. Novel biodegradable and ultra-flexible transparent conductive film for green light OLED devices. *Carbon* **2021**, *172*, 379-389.

(15) Gu, Z. Z.; Tian, Y.; Geng, H. Z.; Rhen, D. S.; Ethiraj, A. S.; Zhang, X.; Jing, L. C.; Wang, T.; Xu, Z. H.; Yuan, X. T. Highly conductive sandwich-structured CNT/PEDOT:PSS/CNT transparent conductive films for OLED electrodes. *Appl. Nanosci.* **2019**, *9*, 1971-1979.

(16) Cai, W.; Zhu, Y.; Li, X.; Piner, R. D.; Ruoff, R. S. Large area few-layer graphene/graphite films as transparent thin conducting electrodes. *Appl. Phys. Lett.* **2009**, *95*, 123115.

(17) Kim, K. S.; Zhao, Y.; Jang, H.; Lee, S. Y.; Kim, J. M.; Kim, K. S.; Ahn, J. H.; Kim, P.; Choi, J. Y.; Hong, B. H. Large-scale pattern growth of graphene films for stretchable transparent electrodes. *Nature* **2009**, *457*, 706-710.

(18) Zhao, J. P.; Pei, S. F.; Ren, W. C.; Gao, L. B.; Cheng, H. M. Efficient Preparation of Large-Area Graphene Oxide Sheets for Transparent Conductive Films. *ACS Nano* **2010**, *4*, 5245-5252.

(19) Becerril, H. A.; Mao, J.; Liu, Z.; Stoltenberg, R. M.; Bao, Z.; Chen, Y. Evaluation of solution-processed reduced graphene oxide films as transparent conductors. *ACS Nano* **2008**, *2*, 463-470.

(20) Green, A. A.; Hersam, M. C. Solution Phase Production of Graphene with Controlled Thickness via Density Differentiation. *Nano Lett.* **2009**, *9*, 4031-4036.

(21) Liang, Y.; Frisch, J.; Zhi, L.; Norouzi-Arasi, H.; Feng, X.; Rabe, J. P.; Koch, N.; Mullen, K. Transparent, highly conductive graphene electrodes from acetylene-assisted thermolysis of graphite oxide sheets and nanographene molecules. *Nanotechnology* **2009**, *20*, 434007.

(22) Li, X. L.; Zhang, G. Y.; Bai, X. D.; Sun, X. M.; Wang, X. R.; Wang, E.; Dai, H. J. Highly conducting graphene sheets and Langmuir-Blodgett films. *Nat. Nanotechnol.* **2008**, *3*, 538-542.

(23) Wang, X.; Zhi, L. J.; Mullen, K. Transparent, conductive graphene electrodes for dye-sensitized solar cells. *Nano Lett.* **2008**, *8*, 323-327.

(24) Liang, Y. Y.; Frisch, J.; Zhi, L. J.; Norouzi-Arasi, H.; Feng, X. L.; Rabe, J. P.; Koch, N.; Mullen, K. Transparent, highly conductive graphene electrodes from acetylene-assisted thermolysis of graphite oxide sheets and nanographene molecules. *Nanotechnology* **2009**, *20*.

(25) Lee, K.; Lee, H.; Shin, Y.; Yoon, Y.; Kim, D.; Lee, H. Highly transparent and flexible supercapacitors using graphene-graphene quantum dots chelate. *Nano Energy* **2016**, *26*, 746-754.

(26) Fan, X.; Chen, T.; Dai, L. Graphene networks for high-performance flexible and transparent supercapacitors. *RSC Adv.* **2014**, *4*, 36996.

(27) Chen, T.; Xue, Y. H.; Roy, A. K.; Dai, L. M. Transparent and Stretchable High-Performance Supercapacitors Based on Wrinkled Graphene Electrodes. *ACS Nano* **2014**, *8*, 1039-1046.

(28) Gao, Y.; Zhou, Y. S.; Xiong, W.; Jiang, L. J.; Mahjouri-samani, M.; Thirugnanam, P.; Huang, X.; Wang, M. M.; Jiang, L.; Lu, Y. F. Transparent, flexible, and solid-state supercapacitors based on graphene electrodes. *APL Mater.* **2013**, *1*, 012101.